Near-field second-harmonic generation of semiconductor quantum dots

Ansheng Liu and Garnett W. Bryant
National Institute of Standards and Technology, Gaithersburg, Maryland 20899
(Received 24 July 1998)

Optical second-harmonic (SH) response of a semiconductor quantum dot (QD) excited by the near field of a tip in a near-field scanning-optical microscope is investigated theoretically. Using an anisotropic effective-mass approximation, we analyze the frequency- and space-dependent SH nonlinear current density in the midgap frequency region associated with interband and intersubband transitions in the QD system. Both heavy- and light-hole states contribute to the SH signal of the QD system. Assuming that an external field drives the tip and the tip field excites the QD, and neglecting local-field effects, we define an effective SH susceptibility tensor of the QD/tip system in terms of the incident-external field. The second-harmonic generation is allowed because the rapidly varying tip field excites the selection-rule breaking transitions in the QD system. For a given size of the metal-coated tip, we performed numerical calculations of the SH susceptibility by scanning the tip and varying the frequency. We show that the SH nonlinearity of the QD/tip system is strongly dependent on the tip position because the overlap integral of the QD envelope wave functions and the tip field is varied by scanning the tip over the QD. Our results also show that the spatial distribution of the tip field is reflected in the tip-position dependence of the SH signal. [S0163-1829(99)07103-9]

I. INTRODUCTION

In a conventional nonlinear optical experiment such as second-harmonic generation (SHG), the nonlinear materials are usually illuminated by a far field (laser beam), and the second-harmonic (SH) signal is also collected in the far-field region. In such a situation, it is well known that second-order optical nonlinear effects are absent in the electric-dipole (local) approximation in materials exhibiting central-inversion symmetry.[1] For a semiconductor quantum-dot (QD) structure with a rectangular-potential profile in three dimensions excited by a far field, the SH nonlinear susceptibility arising from interband and intersubband transitions vanishes in the local approximation because of the definite parity of the wave functions. The same conclusion also holds for symmetric quantum-well and quantum-wire structures. Thus, in order to analyze the second-order nonlinearity in these systems, one has to break the system symmetry by means of the driving field or go beyond the electric dipole approximation to include the nonlocality of the optical response in the analysis. Previously, the far-field optical SHG of a symmetric quantum-well structure associated with intersubband transitions was investigated based on a nonlinear nonlocal response theory.[2] It was shown that it is crucial to take into account the spatial variation of the local field for obtaining a nonzero SH signal from a quantum-well system with a symmetric confined-potential profile. Since the local-field component perpendicular to the quantum-well plane varies rapidly across the quantum well, a significant SH conversion efficiency was predicted in the system.[2]

In this paper we show that, if a symmetric QD is excited by a near field produced by a fiber tip of a near-field scanning optical microscope (NSOM), a second-order nonlinear response is generated in the QD system because the tip field (driving field) varies rapidly over the QD domain. The usual optical-transition selection rules for the SH nonlinear interaction between the driving field and the QD are broken either because of the odd parity of the tip field along the polarization direction of the incident field that excites the tip or because the system symmetry is destroyed when the fiber tip is scanned over the QD. The SH susceptibility is strongly dependent on the relative position between the tip and the QD and the tip-position dependence of the SH signal reflects the spatial distribution of the tip field. We also show that, in the near-field excitation regime, the light-hole states contribute significantly to the SHG of a QD, although it was claimed previously that the light hole contribution to the SHG of a quantum well is negligibly small for far-field excitations because the ratio of the light hole and electron-effective masses is very close to the conduction- to valence-band offset ratio.[3] This is partly due to the fact that the near-field excitation enhances the light-hole transition rate in the QD system[4] because the strong z component of the tip field couples to the light hole (the z direction is perpendicular to the end of the fiber tip). Recently, the possibility of studying nonlinear optical properties of a single molecule trapped in the tip-sample junction with near-field optical characterization methods[5] and wave-mixing near-field optics[6] have been discussed theoretically. The near-field second-harmonic generation from a rough-metal surface[7] and Langmuir-Blodgett films[8] has also been measured experimentally.

The present paper is organized as follows. In Sec. II, we calculate the frequency- and space-dependent SH nonlinear current density of a QD using an anisotropic effective-mass approximation. In our theory, both heavy- and light-hole contributions to the SHG are included. Assuming that the QD structure is excited by the near field of the NSOM tip and the SH signal is collected in the far-field region, we define an effective SH susceptibility tensor for the QD/tip system. To calculate the tip field, we model the metal-coated fiber tip as a thin disk. The tip field is the self-consistent response of the disk to the incident field and is solved by use of the discrete-dipole approximation. In Sec. III, we first present numerical calculations of the tip field and then show

numerous results for the SH susceptibility tensor of a GaAs QD obtained by scanning the tip and varying the frequency. The important role of the tip-field parity and breaking the system symmetry by scanning the tip over the QD in the SH nonlinear response of the QD is discussed. Finally, we give a conclusion in Sec. IV.

II. THEORY

We consider a GaAs QD structure having GaAs layer widths of L_x, L_y, and L_z along the x, y, and z directions, respectively. In the optical-frequency range of interest in this paper, we may assume that optical transitions in the QD system only involve conduction and valence bands near the Brillouin-zone center Γ. In the one-band effective-mass approximation, the wave function of electrons (e), heavy holes (hh), and light holes (lh) can be written as

$$\Psi_{b\alpha}(\mathbf{r}) = u_b(\mathbf{r}) F_\alpha(\mathbf{r}), \quad b = e, hh, lh, \tag{1}$$

where $u(\mathbf{r})$ and $F(\mathbf{r})$ are the periodic Bloch and envelope parts of the wave functions. For simplicity, we adopt, in this paper, the infinite-barrier model to calculate the eigenenergy (E_α) and the corresponding envelope function of electrons and holes, neglecting the band-mixing and electron-hole correlation effects. Therefore, the spatial dependence of the envelope wave function takes a separable form $F_\alpha(\mathbf{r}) = F_x(x) F_y(y) F_z(z)$ where the function $F_i(i = x, y, z)$ represents a standing wave along each coordinate direction. We note that including the finite-barrier height and the heavy- and light-hole band interaction[9] would make quantitative changes in the electronic energies and envelope functions of the QD system compared to the results in the infinite-barrier model, thus would result in quantitative changes in our final results. However, we expect that neglecting these effects in the calculations does not modify qualitatively our results. In calculating hole states, we include the anisotropy of the effective masses for both the heavy- and light-holes. The electron, heavy, and light hole effective mass tensors are given by

$$\vec{m}_e^* = \begin{bmatrix} m_e^* & 0 & 0 \\ 0 & m_e^* & 0 \\ 0 & 0 & m_e^* \end{bmatrix}, \tag{2}$$

$$\vec{m}_{hh}^* = \begin{bmatrix} \dfrac{m_0}{\gamma_1 + \gamma_2} & 0 & 0 \\ 0 & \dfrac{m_0}{\gamma_1 + \gamma_2} & 0 \\ 0 & 0 & \dfrac{m_0}{\gamma_1 - 2\gamma_2} \end{bmatrix}, \tag{3}$$

$$\vec{m}_{lh}^* = \begin{bmatrix} \dfrac{m_0}{\gamma_1 - \gamma_2} & 0 & 0 \\ 0 & \dfrac{m_0}{\gamma_1 - \gamma_2} & 0 \\ 0 & 0 & \dfrac{m_0}{\gamma_1 + 2\gamma_2} \end{bmatrix}, \tag{4}$$

where m_0, m_e^*, and γ_1 and γ_2 are the free-electron mass, the effective-electron mass, and the Luttinger parameters, respectively.

When the QD is excited by a tip field of angular frequency of ω (see Fig. 1), the near field $[\mathbf{E}(\mathbf{r})]$ induces a SH nonlinear current density across the QD system. In a second-order perturbation theory, the frequency- and space-dependent nonlinear current density stemming from combined interband and intersubband transitions is given by[10]

$$\mathbf{J}^{NL}(2\omega, \mathbf{r}) = \frac{1}{\omega^2} \sum_{\sigma,\alpha,\beta,\gamma} \frac{\mathbf{j}_{\alpha\beta}(\mathbf{r}) \left[\int \mathbf{j}_{\beta\gamma}(\mathbf{r}) \cdot \mathbf{E}(\mathbf{r}) d^3r \right] \left[\int \mathbf{j}_{\gamma\alpha}(\mathbf{r}) \cdot \mathbf{E}(\mathbf{r}) d^3r \right]}{\hbar(2\omega + i/\tau) - E_{\alpha\beta}} \left[\frac{f_0(E_\gamma) - f_0(E_\alpha)}{\hbar(\omega + i/\tau) - E_{\alpha\gamma}} - \frac{f_0(E_\beta) - f_0(E_\gamma)}{\hbar(\omega + i/\tau) - E_{\gamma\beta}} \right], \tag{5}$$

where $\mathbf{j}_{\alpha\beta}(\mathbf{r})$ is the one-electron transition-current density between state α and state β, σ represents the spin, f_0 is the electron Fermi-Dirac distribution function, τ is the relaxation time, and $E_{\alpha\beta} \equiv E_\alpha - E_\beta$. Note that we have ignored the band index in Eq. (5) for brevity. We will restore it when it is necessary. For the optical transition between the conduction and valence band, the transition-current density is given, in the envelope-function approximation, by

$$\mathbf{j}_{\alpha\beta}(\mathbf{r}) = -\frac{e}{m_0} \mathbf{P}_{cv} F_\alpha(\mathbf{r}) F_\beta^*(\mathbf{r}), \tag{6}$$

where $-e$ is the electron charge, and $\mathbf{P}_{cv}$ is the interband momentum matrix element at the Brillouin zone *center*. The atomiclike wave functions of the heavy- and light-hole bands at the Γ point, which are needed to evaluate $\mathbf{P}_{cv}$, are[11]

$$|3/2, 3/2\rangle = \frac{1}{\sqrt{2}} |(X + iY)\uparrow\rangle, \tag{7}$$

$$|3/2, 1/2\rangle = \frac{i}{\sqrt{6}} |[(X + iY)\downarrow - 2Z\uparrow]\rangle, \tag{8}$$

$$|3/2,-1/2\rangle=\frac{1}{\sqrt{6}}|[(X-iY)\uparrow+2Z\downarrow]\rangle, \tag{9}$$

$$|3/2,-3/2\rangle=\frac{i}{\sqrt{2}}|(X-iY)\downarrow\rangle, \tag{10}$$

where $|X\rangle,|Y\rangle$, and $|Z\rangle$ are the orbital wave functions of the top of the valence band. $\uparrow$ and $\downarrow$ denote spin-up and spin-down components. The atomic-wave function of the conduction band is constructed by $|1/2,\pm 1/2\rangle=|s\uparrow\downarrow\rangle,|s\rangle$ being the orbital-wave function of the bottom of the conduction band. For the intersubband transition within the conduction and valence bands, the transition-current density reads as

$$\mathbf{j}_{\alpha\beta}(\mathbf{r})=-\frac{e\hbar}{2i\vec{m}_b^*}\cdot[F_\beta^*(\mathbf{r})\nabla F_\alpha(\mathbf{r})-F_\alpha(\mathbf{r})\nabla F_\beta^*(\mathbf{r})],$$

$$b=e,hh,lh. \tag{11}$$

In the present paper we are mainly interested in the case where the fundamental frequency of the incident field is close to the half of the energy gap (E_g). In such a situation, the dominant contribution to the SH nonlinear current density is due to the valence (v)-conduction (c_1)-conduction (c_2)-valence (v) and conduction (c)-valence (v_1)-valence (v_2)-conduction (c) level transitions in the QD system. Note that c's and v's are the abbrevations of quantum numbers (n_x,n_y,n_z) for the states belonging to the conduction and valence bands, respectively. Taking the low-temperature limit and keeping only the resonant term in the expression for the nonlinear current density, it immediately follows from Eq. (5) that

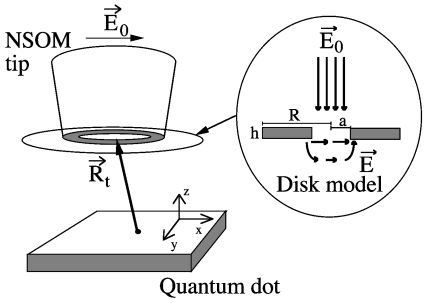

FIG. 1. Schematic diagram showing a QD system excited by a fiber tip in a near-field scanning-optical microscope. The disk model used to calculate the tip field is also indicated.

$$\mathbf{J}^{NL}(2\omega,\mathbf{r})=\frac{1}{\omega^2}\left\{\sum_{\sigma,c,v_1,v_2}\frac{\mathbf{j}_{cv_1}(\mathbf{r})\left[\int\mathbf{j}_{v_1v_2}(\mathbf{r})\cdot\mathbf{E}(\mathbf{r})d^3r\right]\left[\int\mathbf{j}_{v_2c}(\mathbf{r})\cdot\mathbf{E}(\mathbf{r})d^3r\right]}{[\hbar(2\omega+i/\tau)-E_{cv_1}][\hbar(\omega+i/\tau)-E_{cv_2}]}\right.$$
$$\left.-\sum_{\sigma,v,c_1,c_2}\frac{\mathbf{j}_{c_2v}(\mathbf{r})\left[\int\mathbf{j}_{vc_1}(\mathbf{r})\cdot\mathbf{E}(\mathbf{r})d^3r\right]\left[\int\mathbf{j}_{c_1c_2}(\mathbf{r})\cdot\mathbf{E}(\mathbf{r})d^3r\right]}{[\hbar(2\omega+i/\tau)-E_{c_2v}][\hbar(\omega+i/\tau)-E_{c_1v}]}\right\}. \tag{12}$$

As it stands, Eq. (12) shows that the spatial variation of the SH nonlinear current density is determined by the overlap of the conduction- and valence-band envelope wave functions [cf. Eq. (6)], and the strength of the current-density oscillation is controlled by the combined interband and intersubband transitions.

In order to calculate the SH signal, one has to determine the local field $[\mathbf{E}(\mathbf{r})]$ driving the QD system. If we neglect the influence of the interaction between the tip and the QD on the fundamental local field, $\mathbf{E}(\mathbf{r})$ would be the tip field calculated in the absence of the QD system. Here we should mention that in real samples the QD is embedded in barrier materials and the difference between the background dielectric constants for the QD and barrier medium is usually small. Also, including the local-field correction to the tip field arising from the dielectric mismatch between vacuum and the semiconductor-background material changes the composition of the propagating and evanescent components of the tip field, namely a part of the evanescent wave in vacuum is converted into a propagating wave inside the QD structure because the dielectric constant of the QD structure is larger than unity. However, the presence of the background material does not influence the symmetry of the tip-field variation[12] that is important for our analysis of the SHG of a symmetric QD. In the following we will focus our attention on the calculations of the tip field.

Although the experimental techniques of near-field scanning optical microscopy have been developed rapidly in the last few years,[13–20] a realistic and unique model for calculating the tip field of a metal-cladded fiber tip is still lacking. Previously, the Bethe-Bouwkamp model has been used to calculate the tip field and to analyze experimental near-field images.[21] However, in this model the effect of the finite thickness of the metal cladding on the tip field is neglected. Also, the tip has been modeled frequently as a single-radiating dipole[22] for the simplicity of calculations and the clarity of the physical picture. Unfortunately, the single-dipole model cannot account for the dependence of the tip field on tip parameters such as aperture or cladding size. The tip has also been modeled as a series of dipoles distributed throughout the tip volume to model the tip more realistically.[23,24] The self-consistent response of this set of dipoles describes the tip response. However, even with this model, only the response of the end of the tip can be considered. Otherwise, the performance becomes computationally prohibitive. In this paper, we will take this approach. We

model the end of the metal-coated tip as a thin disk of height h and of radius R, as shown in Fig. 1. The interior (core) part of the disk is glass and serves as an aperture (radius a). The remaining part of the tip is aluminum cladding. We assume an incident-plane electromagnetic field ($\mathbf{E}_0$) of frequency ω locally illuminates the core region of the tip. The spatially localized field radiated from the whole tip is the self-consistent response of the tip to the driving field. Our model obviously cannot account for light-propagation effects through the fiber down to the end of the tip. However, it should reproduce the essential features of the field emitted by the tip. The tip-field distribution calculated based on our disk model and the Bethe-Bouwkamp model exhibits essentially the same symmetry. However, our disk model predicts a strong tip-size (metal-cladding thickness) dependence of the tip field that is not described in the Bethe-Bouwkamp model. Our model predicts internal structure in the tip field underneath the metal cladding, as will be shown in Sec. III. This fine structure is responsible for a triplet structure (a central minimum and side maxima) in the transmission NSOM images of Au nanoparticles observed in recent experiments.[25] We have simulated these NSOM images by use of different models, particularly, the disk model and the Bethe-Bouwkamp model. We found that our disk model correctly accounts for the position of the side maxima in the NSOM images as well as the different widths of the central minimum in the NSOM images along the directions parallel and perpendicular to the polarization direction of the light in the far zone. The driving field in a real NSOM tip is not a plane wave but has a maximum amplitude in the core region and decays rapidly inside the metal cladding. In our disk model, a steplike distribution of the driving field (a constant amplitude in the core region and zero inside the metal cladding) is used. We have checked that including a smooth spatial variation of the driving field does not significantly change the tip field, in particular, does not change the symmetry of the tip field at all.

Assuming that the optical response of the tip material is linear and can be characterized by a local isotropic conductivity, we use the Green's function method to determine self-consistently the tip field [$\mathbf{E}(\mathbf{r})$]. Recalling that the tip is excited by an external field $\mathbf{E}_0(\mathbf{r})$, we find the local field by solving the integral equation

$$\mathbf{E}(\mathbf{r})=\mathbf{E}_0(\mathbf{r})-i\mu_0\omega\int \overleftrightarrow{G}(\omega,\mathbf{r},\mathbf{r}')\cdot\sigma(\omega,\mathbf{r}')\mathbf{E}(\mathbf{r}')d^3r', \tag{13}$$

where $\overleftrightarrow{G}$ and $\sigma(\omega,\mathbf{r}')$ are the vacuum dyadic Green's function and the frequency-dependent local conductivity of the tip materials. Because the Green's function possesses a singularity when the source point $\mathbf{r}'$ approaches the observation point $\mathbf{r}$, it is, in general, almost impossible to solve Eq. (13) exactly. In order to obtain an approximate solution to the above equation, we divide the tip into N small subvolumes (V) and replace the integral in Eq. (13) by a summation. Taking an appropriate renormalization procedure to remove the singularity of the Green's function, it follows naturally from Eq. (13) that the local field inside the tip at each grid point $\mathbf{r}_i$ can be obtained from the following algebraic equations

$$\mathbf{E}(\mathbf{r}_i)=\mathbf{E}_0(\mathbf{r}_i)-\mu_0\omega^2\sum_{j\neq i}^{N}\overleftrightarrow{G}(\omega,\mathbf{r}_i,\mathbf{r}_j)\cdot\alpha(\omega,\mathbf{r}_j)\mathbf{E}(\mathbf{r}_j),$$

$$i=1,2,\ldots,N, \tag{14}$$

where

$$\alpha(\omega,\mathbf{r}_j)=3\epsilon_0 V\frac{\epsilon(\omega,\mathbf{r}_j)-1}{\epsilon(\omega,\mathbf{r}_j)+2} \tag{15}$$

is the local-dipole polarizibility of each subvolume, $\epsilon(\omega,\mathbf{r}_j)=1+i\sigma(\omega,\mathbf{r}_j)/(\epsilon_0\omega)$ being the relative dielectric constant of the tip material at the grid point $\mathbf{r}_j$. The approach of solving the local field through Eqs. (14) and (15) is also called the coupled- or discrete-dipole method, which has been widely used in the electromagnetic scattering[26,27] and NSOM problems.[22,28,29] After obtaining the electric field inside the tip, one can also calculate the field [$\mathbf{E}(\mathbf{r})$] radiated from the tip by using Eq. (14), letting $\mathbf{E}_0$ be equal to zero.

Once the tip field has been determined, we can calculate the SH nonlinear current density by using Eq. (12) to evaluate the SHG strength. If we are interested in the SH signal that is observed in the far-field region when the QD is excited by the near field of a tip and neglect local-field effects, then the radiation strength of the SHG is essentially proportional to the square of the integrated nonlinear current density or polarization. Therefore, it is physically meaningful to define an effective susceptibility tensor ($\overleftrightarrow{\chi}$) of the QD system via

$$\frac{i}{2\omega}\frac{1}{L_xL_yL_z}\int \mathbf{J}^{NL}(2\omega,\mathbf{r})d^3r=\epsilon_0\overleftrightarrow{\chi}:\mathbf{E}_0\mathbf{E}_0. \tag{16}$$

Here we emphasize that $\mathbf{E}_0$ is the amplitude of the incident field that *drives* the fiber tip, not the tip field that drives the QD. Therefore, the effective susceptibility defined above may be viewed as a measure of the optical nonlinearity of the QD/tip system. From such a point of view, one should expect that the SH susceptibility of the QD system is strongly dependent on the tip position. In particular, we will show that varying the tip position breaks the symmetry of the QD/tip system and leads to a nonzero component of the SH susceptibility tensor that otherwise would be zero for the far-field excitation in the electrical-dipole approximation.

III. NUMERICAL RESULTS

In this section we present a numerical study of the nonlinear near-field optical response of a QD system. To this end we first analyze the tip field that excites the optical transitions in the QD. Using the coupled-dipole method described in the preceding section, we calculated the tip field as a function of the space coordinate. In Figs. 2–4 are shown the tip-field variations in the xy plane 20 nm away from the end of the tip. In the calculations, we assume the external field of wavelength $\lambda=1300$ nm is polarized along the x axis and has unit amplitude. The disk-tip geometry used in the calculations is given as follows: the disk-tip height is $h=14$ nm, the total-tip radius is $R=147$ nm, and the aperture radius is $a=49$ nm. Note that we choose a small value for the disk height h for the convenience of calculations. This model has been used to accurately simulate experimental

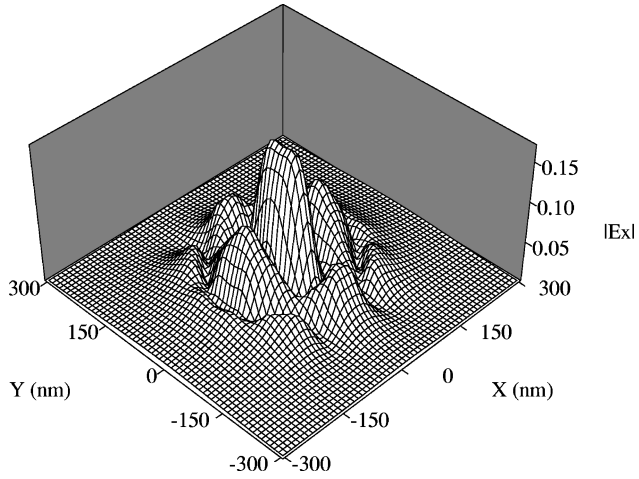

FIG. 2. Magnitude of the x component of the tip field as a function of the space coordinate in the xy plane 20 nm away from the end of the tip. The disk tip height is 14 nm, the total tip radius is 147 nm, and the core radius is 49 nm. The wavelength is 1300 nm.

NSOM images of Au particles.[25] We have performed numerical calculations of the tip field for different values of the disk height h. We found that increasing the disk height only makes a small change in the tip-field distribution (detailed calculations of the tip field and comparisons of results obtained by different methods will be presented in a forthcoming paper). It appears from Figs. 2–4 that the tip field (all three components) varies rapidly in space and is highly localized near the aperture. In the vicinity of the tip edge there is also a significant portion of the field due to the large dielectric mismatch between the metal coating and vacuum. For the x component of the field, a local maximium occurs underneath the aluminum cladding layer for the same reason. This additional internal structure in the tip field is not predicted in the Bethe-Bouwkamp model but has been detected experimentally.[25] We also found that more internal structure in the tip field appears when the thickness of the metal cladding is increased. Far away from the tip all three components of the field decay rapidly. Also, we note from Figs. 2–4 that

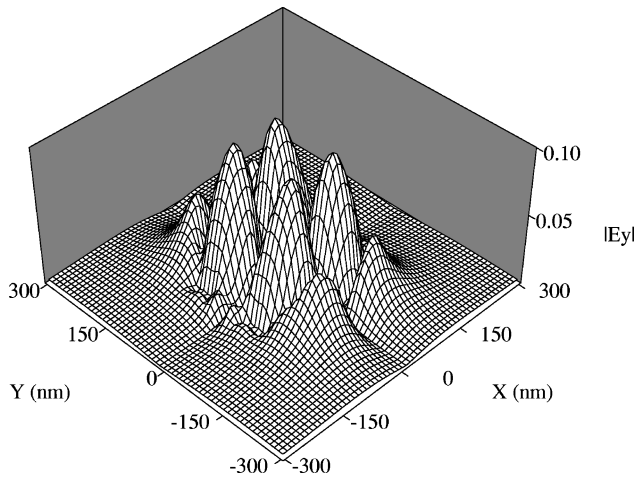

FIG. 3. Magnitude of the y component of the tip field as a function of the space coordinate in the xy plane 20 nm away from the end of the tip. The same parameters are used as in Fig. 2.

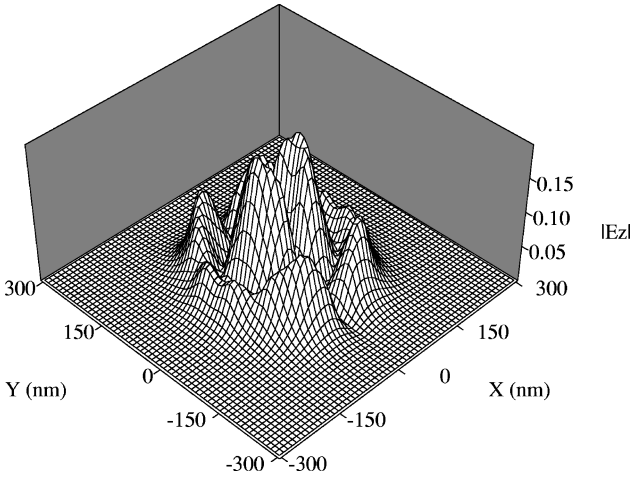

FIG. 4. Magnitude of the z component of the tip field as a function of the space coordinate in the xy plane 20 nm away from the end of the tip. The same parameters are used as in Fig. 2.

the x and z components of the tip field are larger than the y component. This implies that the y component of the SH nonlinear current density would be smaller than the other two components when the tip is excited by an external field polarized along the x axis.

We now investigate how the tip position influences the SHG of the QD system. In the following calculations, we also assume that the external field is polarized along the x axis. In this case, the relevant elements of the SH susceptibility tensor of our QD/tip system defined in Eq. (16) are χ_{xxx}, χ_{yxx}, and χ_{zxx}, which correspond to the integrated SH nonlinear current density along the x, y, and z directions, respectively. Since χ_{yxx} is very small when the tip is scanned along the x and y axes due to the small y component of the tip field (cf. Fig. 3), we shall not consider it in our numerical analyses. The tip size and geometry are the same as used in Figs. 2–4. We scan the tip along the x or y direction over the QD at the distance of 20 nm between the tip end and the top of the QD. Thus, when the tip position is at $x=0$ and $y=0$, the center of the QD is just underneath the center of the tip. The material parameters for the GaAs QD used in the calculations are $L_x=50$ nm, $L_y=10$ nm, $L_z=5$ nm, $m_e^*=0.067m_0$, $\gamma_1=6.85, \gamma_2=2.1$, and $\hbar/\tau=10$ meV. We choose the above-mentioned QD geometry to limit the optical-intersubband transitions contributing to the SH susceptibility to only those among the quantized states confined along the x direction. We do this to simplify the numerical calculations. However, it should be kept in mind that the interband transition involves the states connected with the confinement along all the three directions. In Figs. 5 and 6 we show, respectively, the xxx and zxx components of the effective SH susceptibility tensor as a function of the tip position along the x axis at different fundamental frequencies. Note that, in our calculations, we have only taken into acount the contribution to the SHG from 15 quantum (e,hh, and lh) states near the bottom of the conduction band and the top of the valence band. This should be justified in the frequency range used in Figs. 5 and 6. The eigenenergies of these quantum states are listed in Table I. Also, it should be stressed that both heavy- and light-hole states contribute to the xxx component of the susceptibility. Owing to the inter-

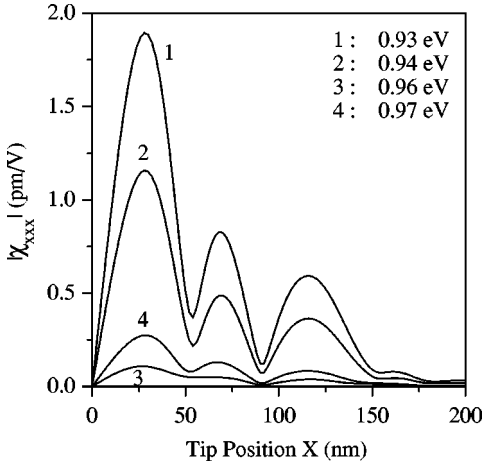

FIG. 5. Magnitude of the *xxx* component of the effective SH susceptibility tensor of a QD with $L_x=50$ nm, $L_y=10$ nm, and $L_z=5$ nm when a tip is scanned along the *x* direction over the QD at a height of 20 nm. The tip field is calculated based on a disk model described in the text. The fundamental photon energies of $\hbar\omega=0.93$ (curve 1), 0.94 (curve 2), 0.96 (curve 3), and 0.97 eV (curve 4) are used.

band momentum matrix element, however, the *zxx* component of the susceptibility is solely due to the light-hole transitions. It appears from Figs. 5 and 6 that the SH nonlinearity of the QD strongly depends on not only the frequency but also the relative position between the tip and the QD. The tip-position dependence of the SHG is ascribed to the overlap of the local-tip field and the QD envelope-wave functions, which determines the magnitude of the nonlinear current-density oscillation. Thus, it is not surprising that the SH susceptibility vanishes as the tip is scanned far from the QD. Also, it is interesting to note from Fig. 5 that the *xxx* component of the susceptibility tensor is very small when the QD is underneath the tip, although the tip field within the domain over which the QD wave functions extend is relatively large. This is so because the *xxx* component of the susceptibility is mainly induced by the *x* component of the tip field. Because of the symmetry of the QD wave functions

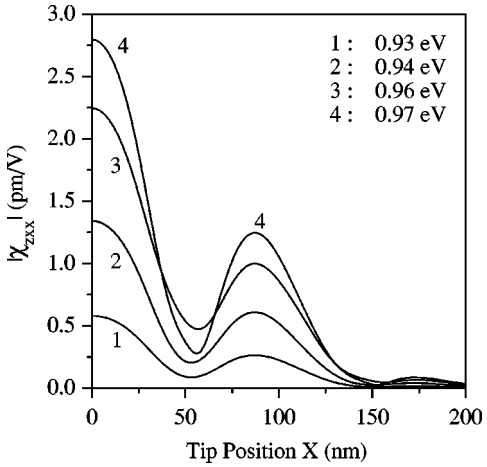

FIG. 6. Magnitude of the *zxx* component of the effective SH susceptibility tensor of a QD with $L_x=50$ nm, $L_y=10$ nm, and $L_z=5$ nm when a tip is scanned along the *x* direction over the QD at a height of 20 nm. The same parameters are used as in Fig. 5.

TABLE I. Eigenenergies of a GaAs QD with $L_x=50$ nm, $L_y=10$ nm, and $L_z=5$ nm.

Quantum numbers (n_x,n_y,n_z)	E_e (eV)	E_{hh} (eV)	E_{lh} (eV)
1,1,1	1.7069	−0.0749	−0.1848
2,1,1	1.7136	−0.0789	−0.1869
3,1,1	1.7248	−0.0856	−0.1905
4,1,1	1.7406	−0.0951	−0.1955
5,1,1	1.7608	−0.1072	−0.2019

and the *x* component of the tip field, the SH signal is expected to be small in this case. (In fact, when the tip position is at $x=0$ and $y=0$, $\chi_{xxx}=0$ because of the definite parity of the wave functions and the tip field.) We also note from Fig. 5 that there exists a pronounced maximum when the tip is scanned somewhat away from the QD. This enhancement in the SH nonlinearity is due to breaking the symmetry of overlap of the wave function and the tip field. When the tip is further scanned away from the QD, two additional small peaks appear in the *xxx* component of the susceptibility. These peaks are due to the combined *x* and *z* components of the tip-field enhancement as shown in Figs. 2 and 4 for $x=70$ and 120 nm and two minima occur for $x\approx 50$ and 90 nm. The two minima occur when the field distribution about the center of the dot is locally approximately symmetric. For $x\approx 50$ nm, this occurs when the edge of the aperture is centered on the dot. For $x\approx 90$ nm, it occurs when the structure under the cladding is centered on the dot. This result suggests that the nonlinear near-field microscopy of quantum nanostructures may provide an effective probe of the tip field.

In contrast to the *xxx* component, the *zxx* component of the SH susceptibility shows a rather different tip-position dependence, as can be seen in Fig. 6. Particularly, we note from Fig. 6 that χ_{zxx} reaches its maximum value when the tip is just over the QD. This is because, when the tip position is close to zero, the *z* component of the tip field dominates the contribution to the *zxx* element of the susceptibility, although the *x* component of the tip field also contributes to χ_{zxx} through the field-induced intersubband transitions within the conduction and valence bands. Since the *z* component of the tip field has odd parity along the *x* axis compared to the even parity for the *x* component of the tip field, the overlap integral of the wave functions and the *z* component of the tip field has a maximum value when the tip and the QD are centered. This field component is very weak in the far-field excitation and would not generate significant SH signal in that case. One also sees from Fig. 6 that an additional small peak appears when the tip position is about $x=87$ nm. This occurs when the enhanced field under the cladding is centered on the dot.

From Figs. 5 and 6 we also observe the strong frequency dependence of the magnitude of the SH susceptibility. The *xxx* component of the susceptibility has a large magnitude when the photon energy is about $\hbar\omega=0.93$ eV. This is because, in the vicinity of this frequency, resonant two-photon optical transitions occur between one of the heavy-hole states and one of the electron states ($2\hbar\omega\approx E_{e\text{-}hh}$). At the higher frequency (say $\hbar\omega=0.97$ eV), the *zxx* component of the susceptibility reaches a high value since the fundamental

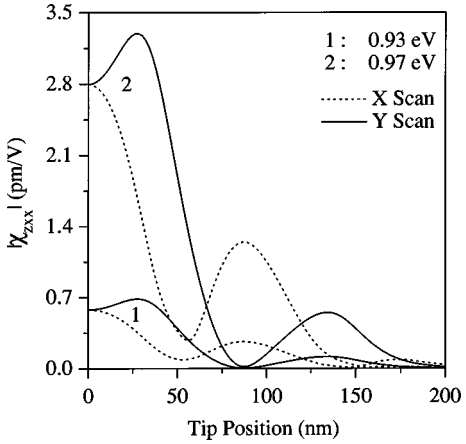

FIG. 7. Comparison of the results for the zxx component of the SH susceptibility of a QD system with $L_x=50$ nm, $L_y=10$ nm, and $L_z=5$ nm when the tip is scanned along the x (dotted curves) and y (solid curves) directions at a height of 20 nm over the QD. The two different fundamental frequencies, i.e., $\hbar\omega=0.93$ (labeled 1) and 0.97 eV (labeled 2) are used in the calculations.

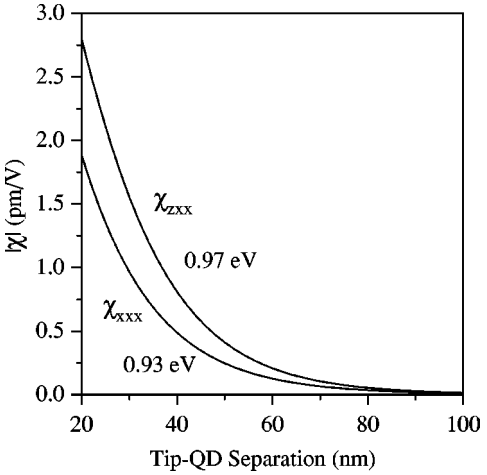

FIG. 8. Magnitude of the xxx and zxx components of the SH susceptibility tensor of a QD system with $L_x=50$ nm, $L_y=10$ nm, and $L_z=5$ nm as a function of the tip-QD separation. In calculating χ_{xxx}, the tip is located at $x=30$ nm and $y=0$ in the xy plane, and the photon energy is $\hbar\omega=0.93$ eV. In the calculations of χ_{zxx}, the tip is placed at $x=0$ and $y=0$ in the xy plane, and a photon energy of $\hbar\omega=0.97$ eV is employed.

two-photon energy is near one of the resonant light-hole electron-transition energies ($2\hbar\omega\approx E_{e\text{-}lh}$). A detailed discussion of the frequency dependence of the SH susceptibility will be presented later. The tip-position dependence of the SH signal is essentially independent on the frequency (cf. Figs. 5 and 6).

It is also interesting to analyze the modification of the SH signal when the tip is scanned along the y direction, while the polarization of the external field is still along the x axis. In this case, one would expect that the tip-position dependence of the SH susceptibility tensor along the y axis is different from that along the x axis because the spatial distribution of the tip field is different in the two coordinate directions (cf. Figs. 2 and 4). Figure 7 compares the results for the zxx component of the SH susceptibility of a QD system with $L_x=50$ nm, $L_y=10$ nm, and $L_z=5$ nm when the tip is scanned along the x (dotted curves) and y (solid curves) directions at a tip-QD separation of 20 nm. The two different fundamental frequencies, i.e., $\hbar\omega=0.93$ and 0.97 eV are used in the calculations. We see from Fig. 7 that, although the main features of the tip-position dependence of the SH signal are similar along the x and y axes, obvious differences exist for the two cases. Particularly, one notes that the SH susceptibility first increases and then decreases as the tip is scanned along the y axis, and the decrease of the SH signal with the tip scanning along the y axis is thus slower than that along the x axis because both x and z components of the tip field in the core region exhibit the same behavior (cf. Figs. 2 and 4). The initial increase arises because increasing y increases the amount of the edge that overlaps the dot. Also, the second peaks in the tip-position dependence of the SH signal appear in different locations along the different directions. This is also due to the asymmetric distribution of the tip field in the xy plane because the polarization of the incident field is along the x axis. We have also calculated the xxx component of the SH susceptibility when the tip is scanned along the y axis. Our calculations indicate that χ_{xxx} is equal to zero because the symmetry of the overlap of the QD wave function and the x component of the tip field is not broken as the tip is scanned along the y axis.

Now let us study the change of the SH signal when the tip is pulled away from the QD along the z direction. In Fig. 8 we plot the xxx and zxx components of the SH susceptibility as a function of the tip-QD separation. In calculating χ_{xxx}, we placed the tip at $x=30$ nm and $y=0$, and used the photon energy of $\hbar\omega=0.93$ eV. In the calculations of χ_{zxx}, the tip was at $x=0$ and $y=0$ in the xy plane, and a photon energy of $\hbar\omega=0.97$ eV was employed. We see from Fig. 8 that the magnitude of the SH susceptibility decays exponentially with an increase in the tip-QD separation because of the decay of the tip field that excites the optical transitions in the QD. The decay length for the xxx and zxx components of the SH susceptibility is estimated to be about 15 nm, which corresponds to the decay length of the square of the tip field at the fundamental frequency. Since the SH signal detected in the far-field region is proportional to the square of the susceptibility, it is expected that the SH intensity decays two times faster.

At this stage, we remind ourselves that all results presented in Figs. 5–8 are obtained for a fixed *large* line broadening of 10 meV. For high-quality QD structures, the linewidth is much smaller and can be as small as 0.14 meV.[30] Thus, the calculations discussed so far may underestimate the magnitude of the SH susceptibility. To obtain a reasonable estimate of the maximium SH nonlinearity of our QD system, we calculated the SH susceptibility for different relaxation times by varying the fundamental photon energy. Typical results are shown in Figs. 9 and 10. We see from Figs. 9 and 10 that both the xxx and zxx components of the SH susceptibility are greatly enhanced when the linewidth changes from 5 to 1 meV. A maximum value of about 22 pm/V is obtained for χ_{xxx} when the two-photon energy exactly hits one of the heavy-hole electron interband transition resonances. For the zxx component, an even higher value (about 45 pm/V) is obtained when one of the light-hole elec-

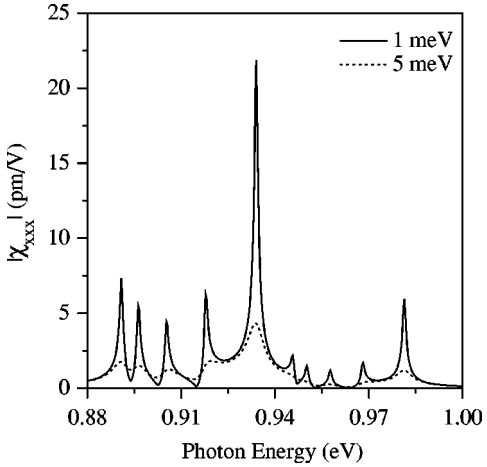

FIG. 9. Magnitude of the *xxx* component of the SH susceptibility tensor of a QD system with $L_x=50$ nm, $L_y=10$ nm, and $L_z=5$ nm as a function of the fundamental photon energy $\hbar\omega$ for two different linewidths, i.e., $\hbar/\tau=1$ (solid line) and 5 meV (dotted line). In the calculations, the tip is located at $x=30$ nm and $y=0$ in the *xy* plane, and tip-QD separation along the *z* direction is 20 nm.

tron interband transitions is resonantly excited (cf. Fig. 10). This result suggests that the light-hole contribution to the SHG of a symmetric QD is significantly enhanced through the near field excitation because of the odd parity of the *z* component of the tip field along the *x* axis. This result is also consistent with the prediction that the near-field excitation enhances the light-hole transition rate in a QD structure.[4] Comparing our results with previous calculations for GaAs quantum wells given in Ref. 3 and noticing the different definition of the SH susceptibility in our case [see Eq. (16) and the sentence below this equation], we find that the magnitude of the SH nonlinearity of the QD is comparable to that for the quantum wells. [Since the tip field in the disk model is about one order of magnitude smaller than the external field that drives the tip (cf. Figs. 2–4), to compare with the results in Ref. 3 the SH susceptibility defined in Eq. (16) should be multiplied by a factor of ~ 100.]

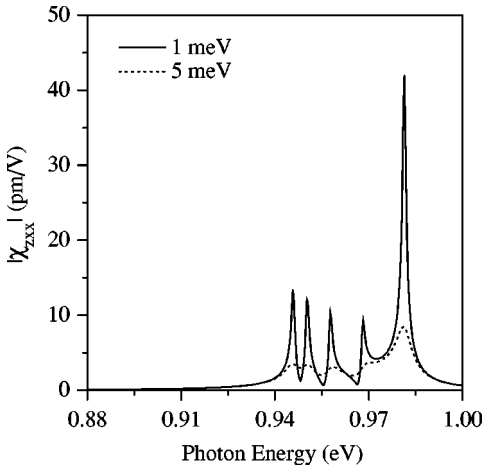

FIG. 10. Magnitude of the *zxx* component of the SH susceptibility tensor of a QD system with $L_x=50$ nm, $L_y=10$ nm, and $L_z=5$ nm as a function of the fundamental photon energy $\hbar\omega$ for two different linewidths, i.e., $\hbar/\tau=1$ (solid line) and 5 meV (dotted line). In the calculations, the tip is located at $x=0$ and $y=0$ in the *xy* plane, and tip-QD separation along the *z* direction is 20 nm.

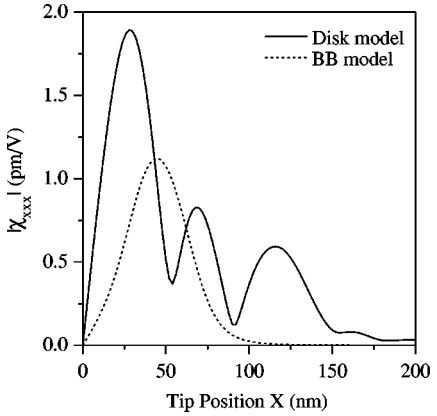

FIG. 11. Comparison of results for the *xxx* component of the SH susceptibility of a QD system with $L_x=50$ nm, $L_y=10$ nm, and $L_z=5$ nm at the fundamental frequency of $\hbar\omega=0.93$ eV when the tip field is calculated based on the disk model (solid curve) and the Bethe-Bouwkamp (BB) model (dotted curve). The same parameters are used as in Figs. 5 and 6.

Finally, we compare in Figs. 11 and 12 the results for the SH susceptibility obtained by using the disk model and the Bethe-Bouwkamp model to calculate the tip field. In the calculations, the same parameters are used as in Figs. 5 and 6 except that a fundamental frequency of $\hbar\omega=0.93$ eV is employed. Note that, in the Bethe-Bouwkamp model,[4,21,31,32] the tip core is vacuum and the metal cladding is a perfect conductor with infinite extension in the *xy* plane but zero extension along the *z* direction. We see from Figs. 11 and 12 that the magnitude and the tip-position dependence of the SH susceptibility are quite different when the tip field is calculated by use of different models. Because there is no fine structure in the spatial distribution of the *x* component of the tip field in the Bethe-Bouwkamp model, the *xxx* component of the SH susceptibility exhibits only one maximum when the tip is scanned away from the center of the QD to break the symmetry. Also, since the space dependence of the *z* component of the tip field in the Bethe-Bouwkamp model differs significantly from that in the disk model, the *zxx* component of the SH susceptibility shows a different tip-position dependence. Structures in the tip-position dependence of the SHG are related to profile in the tip field that are

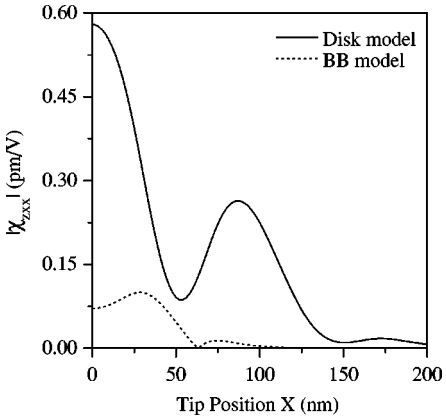

FIG. 12. Same as in Fig. 11 except that the *zxx* component of the SH susceptibility is plotted.

locally approximately symmetric or antisymmetric. This structure can be used to identify the best model for the tip field. Figures 11 and 12 also show that, while the fine structure in the line scans of the SH signal is strongly dependent on the specific model for the tip field, the tip-field symmetry dependence of the SH susceptibility tensor is the same for different models.

IV. CONCLUSION

In this paper we present a theoretical investigation of the nonlinear SH optical response of a QD system excited by a tip field in a near-field optical microscope. By modeling the metal-coated tip as a thin disk consisting of a glass core and a metal-cladding layer, we calculate the tip field by use of the discrete-dipole approximation. Assuming that the tip field drives the optical transitions in the QD system, we calculate the effective SH susceptibility tensor of the QD in the midgap-frequency range. For a given size of the metal-coated tip, we performed numerical calculations of the SH susceptibility by varying the tip position and the fundamental frequency. Our numerical results show that the SH nonlinearity of the QD/tip system is strongly dependent on the tip position because the overlap integral of the QD envelope wave functions and the tip field that determines the strength of the SH nonlinear current oscillations is varied by scanning the tip over the QD. Since the x and z components of the tip field have opposite parities along the x axis, the xxx and zxx components of the SH susceptibility tensor exhibit a quite different tip-position dependence. When the QD and the tip are centered, the xxx component of the SH susceptibility is zero due to the even parity of the x component of the tip field, whereas the zxx component reaches its maximum value because of the odd parity of the z component of the tip field that couples to the light-hole transitions. The maximum value of the xxx component of the susceptibility is obtained when the system symmery is broken by scanning the tip away from the QD. Our results also show that symmetry parities in the tip-field distribution correlate with structures in the tip-position dependence of the SH signal. Using near-field microscopy to generate nonlinear optical response should provide an effective probe of quantum nanostructures and, at the same time, provide additional information about symmetry points in the tip field.

[1] Y. R. Shen, *The Principle of Nonlinear Optics* (Wiley, New York, 1984).
[2] A. Liu and O. Keller, Phys. Rev. B **49**, 13 616 (1994).
[3] A. Fiore, E. Rosencher, B. Vinter, D. Weill, and V. Berger, Phys. Rev. B **51**, 13 192 (1995).
[4] G. W. Bryant, Appl. Phys. Lett. **72**, 768 (1998).
[5] J. M. Vigoureux, C. Girard, and F. Depasse, J. Mod. Opt. **41**, 49 (1994).
[6] X. Zhao and R. Kopelman, Ultramicroscopy **61**, 69 (1995).
[7] I. I. Smolyaninov, A. V. Zayats, and C. C. Davis, Phys. Rev. B **56**, 9290 (1997).
[8] S. I. Bozhevolnyi and T. Geisler, J. Opt. Soc. Am. A **15**, 2156 (1998).
[9] P. C. Sercel and K. J. Vahala, Phys. Rev. B **42**, 3690 (1990).
[10] O. Keller, Phys. Rev. B **33**, 990 (1986).
[11] R. People and S. K. Sputz, Phys. Rev. B **41**, 8431 (1990).
[12] A. Knorr, B. Hanewinkel, H. Giessen, and S. W. Koch, *Theory for Semiconductor Near-Field Optics: Selection Rules and Coherent Spatio-Temporal Dynamics*, Festkörperprobleme/ Advances in Solid State Physics **38** (Vieweg, Braunschweig, in press).
[13] *Near Field Optics*, edited by D. W. Pohl and D. Courjon (Kluwer, Dordrecht, 1993).
[14] E. Betzig and R. J. Chichester, Science **262**, 1422 (1993).
[15] D. Courjon and C. Bainier, Rep. Prog. Phys. **57**, 989 (1994).
[16] R. D. Grober, T. D. Harris, J. K. Trautman, E. Betzig, W. Wegscheider, L. Pfeiffer, and K. West, Appl. Phys. Lett. **64**, 1421 (1994).
[17] R. X. Bian, R. C. Dunn, X. S. Xie, and P. T. Leung, Phys. Rev. Lett. **75**, 4772 (1995).
[18] F. Flack, N. Samarth, V. Nikitin, P. A. Crowell, J. Shi, J. Levy, and D. D. Awschalom, Phys. Rev. B **54**, R17 312 (1996).
[19] A. Richter, G. Behme, M. Süptitz, Ch. Lienau, T. Elsaesser, M. Ramsteiner, R. Nötzel, and K. H. Ploog, Phys. Rev. Lett. **79**, 2145 (1997).
[20] P. A. Crowell, D. K. Young, S. Keller, E. L. Hu, and D. D. Awschalom, Appl. Phys. Lett. **72**, 927 (1998).
[21] G. W. Bryant, E. L. Shirley, L. S. Goldner, E. B. McDaniel, J. W. P. Hsu, and R. J. Tonucci, Phys. Rev. B **58**, 2131 (1998).
[22] L. Novotny, J. Opt. Soc. Am. A **14**, 105 (1997).
[23] B. Hanewinkel, A. Knorr, P. Thomas, and S. W. Koch, Phys. Rev. B **55**, 13 715 (1997).
[24] A. Knorr, F. Steininger, B. Hanewinkel, S. Kuckenburg, P. Thomas, and S. W. Koch, Phys. Status Solidi B **206**, 139 (1998).
[25] L. J. Richter, C. E. Jordan, R. R. Cavanagh, G. W. Bryant, A. Liu, S. J. Stranick, C. D. Keating, and M. J. Natan (unpublished).
[26] B. T. Draine and P. J. Flatau, J. Opt. Soc. Am. A **11**, 1491 (1994).
[27] S. B. Singham and C. F. Bohren, J. Opt. Soc. Am. A **5**, 1867 (1988).
[28] C. Girard, A. Dereux, O. J. F. Martin, and M. Devel, Phys. Rev. B **50**, 14 467 (1994).
[29] C. Girard and A. Dereux, Rep. Prog. Phys. **59**, 657 (1996).
[30] W. Heller, U. Bockelmann, and G. Abstreiter, Phys. Rev. B **57**, 6270 (1998).
[31] H. A. Bethe, Phys. Rev. **66**, 163 (1944).
[32] C. J. Bouwkamp, Philips Res. Rep. **5**, 321 (1950); C. J. Bouwkamp, *ibid.* **5**, 401 (1950).